Isomeric and collective structures in neutron-rich hafnium isotopes

F. Amirzadeh and A. Kardan[*]

School of Physics, Damghan University, P.O. Box 36716-41167, Damghan, Iran

P. M. Walker [†]

Department of Physics, University of Surrey, Guildford, Surrey GU2 7XH, United Kingdom

Hai-Liang Ma

China Institute of Atomic Energy, P.O. Box 275-10, Beijing 102413, China

The structures of isomeric and collective states in neutron-rich hafnium isotopes have been investigated within the paired cranked Nilsson-Strutinsky-Bogoliubov (CNSB), and the unpaired cranked Nilsson-Strutinsky (CNS) formalisms. We show that by combining these two models, a good understanding of the formation of multiquasiparticle prolate isomers is achieved. The calculations show at angular momenta $I \geqslant 35$, well-deformed oblate collective rotation strongly competes energetically with the prolate noncollective states. Comparison is made with experimental data, where available, and with other model calculations.

I. INTRODUCTION

A nuclear isomer is an excited state of a nucleus with a long half-life, in the range nanoseconds to years [1]. It is a quasistable quantum state with a half-life that is at least several orders of magnitude longer than typical half-lives of excited states. The study of isomers can be helpful in exploring the structure of unusual excited states in nuclei, the nuclear mean-field potential, proton-neutron coupling effects, and nuclear shapes [2–4]. The theoretical understanding of nuclear isomers was first introduced by von Weizsäcker in 1936, suggesting that the combination of a large change in the angular momentum and a low energy in an electromagnetic transition can lead to a transition with a long half-life [2,3,5]. The lifetime τ of a nuclear state decaying by a single transition, depends on the transition energy ΔE and the change in the quantum numbers between the isomeric state itself and the state to which it decays [3],

$$1/\tau \propto |\langle f \mid T_\lambda \mid i \rangle|^2 (\Delta E)^{2\lambda+1},$$

where T_λ is the transition operator between the initial and final states and λ is the multipole order of the electromagnetic transition. A high-K isomer is one of the most well-known types of nuclear isomer, which occurs from violation of the electromagnetic transition selection rule requiring that $\lambda \geqslant \Delta K$, where the quantum number K is the projection of the total angular momentum on the symmetry axis, i.e., the sum of all projections of the angular momenta of unpaired nucleons along the symmetry axis, $K = \sum \Omega_i$. A significant difference in K values and a violation of this selection rule led to "forbidden" decay from the high-K isomer to the rotational states of a low-K band, and thus a long half-life for the nuclear excited state [6,7]. A high K value, a relatively low excitation energy, and a well-deformed axially symmetric shape are effective factors resulting in a long half-life for an excited state [8].

In even-even deformed nuclei at low spins, the lowest energy rotational sequence is based on the fully paired ground state. With increasing angular momentum, the collective excitations lead to the breaking of nucleon pairs, and the unpaired nucleons can couple their angular momentum projections Ω along the symmetry axis, thereby forming two-quasiparticle configurations which compete to form the yrast line. However, the situation is more complex if there are high-j nucleons which are coupled through Coriolis effects, so that they can align their intrinsic angular momenta with the collective rotation axis, perpendicular to the symmetry axis [3,6,9]. Nevertheless, when nucleon pairs are broken and recoupled at high spin with a minimal energy cost, they can result in yrast traps, forming long-lived, high-spin isomeric states [1].

In the mass $A \approx 180$ region, there are well-deformed axially symmetric nuclei with many high-Ω orbits close to the neutron and proton Fermi surfaces, and multiquasiparticle states with high-K values can be formed. These states and their rotational bands can compete to form the yrast line [3,6,10–12]. The bandhead decays often need a big change in the K quantum number to occur, and therefore K-forbidden transitions and long half-lives will occur. For example, the $K^\pi = 16^+$, 31-yr isomer of ^{178}Hf is one of the most interesting, arising from a four-quasiparticle configuration [1,13,14]. Predictions for the $Z = 72$ hafnium isotopes indicate a continuation of the well-known high-K isomers into the neutron-rich

---
[*]Corresponding author: aakardan@du.ac.ir

[†]p.walker@surrey.ac.uk

region [1,8,15], and this is an active area of experimental investigation [16,17].

The purpose of the present work is to describe and analyze the features of the isomeric states of even-even hafnium isotopes within the unpaired Cranked Nilsson-Strutinsky (CNS) [18–20] and paired cranked Nilsson-Strutinsky-Bogoliubov (CNSB) [21,22] theoretical formalisms. The results presented here aim to reproduce and complement the current information on the structure of hafnium isomers. However, specifically at low and medium spins, the CNS formalism suffers from the absence of pairing. This problem is overcome with the CNSB method, where the calculations are done in a mesh covering both the deformation space and the pairing space. In the present work, shapes and energies are calculated and compared with total Routhian surface (TRS) and configuration-constrained Woods-Saxon-Strutinsky calculations, as well as with existing data. The overall success establishes the CNSB method as being good for such calculations, and will lead on to further work. This formalism is based on the ultimate cranker method [23] that was applied to the hindrance factor calculation in the decay of the $K = 25$ isomer in ^{182}Os [24].

The paper is organized as follows. The theoretical frameworks of the cranked Nilsson-Strutinsky (CNS) and cranked Nilsson-Strutinsky-Bogoliubov (CNSB) approaches are presented in Sec. II. The results of the calculations of the isomeric states in ^{178}Hf obtained within these two approaches as well as a detailed comparison of these results with experiment are reported in Sec. III. The results for heavier even-even hafnium isotopes are presented in Sec. IV. The shape evolution, with increasing angular momentum as well as with neutron number, is discussed in Sec. V. Finally, all results are summarized in Sec. VI.

II. THEORETICAL FRAMEWORKS

In this section we give a brief introduction to the paired and unpaired cranked Nilsson-Strutinsky approaches. Note that the cranking method discussed is based on the one-dimensional cranking approximation. In the cranking model, the rotation degree of freedom enters in the same way as the deformation degree of freedom. In this system, the nucleons move independently in a rotating nuclear potential [25]. In the unpaired cranked Nilsson-Strutinsky (CNS) formalism, the mean-field Hamiltonian is taken as [19]

$$H = H_{\mathrm{MHO}}(\varepsilon_2, \gamma, \varepsilon_4) - \omega j_x, \quad (1)$$

where H_{MHO} is the modified harmonic-oscillator Hamiltonian and ωj_x describes the cranking around the principal x axis with rotational frequency ω. The diagonalization of the Hamiltonian of Eq. (1) in the rotating basis (see Ref. [25]) gives the eigenvalues, i.e., the single-particle energies, in the rotating frame as a function of axial and triaxial quadrupole and hexadecapole deformation parameters, $e_i^\omega(\varepsilon_2, \gamma, \varepsilon_4)$ for each ω value. The total single-particle energies are calculated by summing the proton and neutron single-particle energies. The total energy of a configuration consists of a macroscopic part which is obtained from the Lublin-Strasbourg drop (LSD) model [26] and a microscopic part calculated with the

Strutinsky shell-correction model [27]. As pointed out above, the calculations are performed in the lattice of deformation ($\varepsilon_2, \gamma, \varepsilon_4$).

The cranked Nilsson-Strutinsky-Bogoliubov (CNSB) model uses the same modified oscillator potential as the CNS model, plus a monopole pairing term as in [21]

$$H = H_{\mathrm{MHO}}(\varepsilon_2, \gamma, \varepsilon_4) - \omega j_x - \Delta(P^\dagger + P) - \lambda \hat{N}, \quad (2)$$

where the two last terms denote the pairing Hamiltonian, and $P^\dagger$ (P) and $\hat{N}$ are the pair creation (annihilation) and the particle number operators. In this procedure, the microscopic energy, after particle number projection, is minimized relative to the pairing parameters, Fermi energy λ, and pairing gap Δ, as well as the deformation parameters. Because the particle-number projection is employed, the pairing strength G is reduced by a factor of 0.95 for the pairing self-consistent calculation [28]. The standard parameters [19] are used in both paired and unpaired calculations.

As seen in Eq. (1), pairing correlations are neglected in the CNS calculations. The absence of the pairing in addition to the simplicity of the modified oscillator potential (see Ref. [29]) makes it possible to fix the structure of configurations. However, it turns out to be questionable to use the CNS formalism at low spins where neglecting the pairing reveals somewhat high discrepancies. However, the CNSB formalism including the pairing correlations is successful in reproducing more properties of isomers which are often observed at low spins. Therefore, we use the paired and unpaired formalisms in parallel to compensate for the deficiencies.

In the CNS and CNSB formalisms, a "diabatic" technique to obtain wave functions with a smooth dependence on the Hamiltonian parameters is employed [23]. The primary advantage of the use of such a method is that it becomes feasible to display the results as function of spin rather than rotational frequency [28]. This is an advantage over the TRS model where the results are presented as function of the rotational frequency which is not a measurable parameter experimentally.

In the present work, to get the gyromagnetic factors, we use the following formula in the CNSB model,

$$g(I) = \frac{\langle \hat{\mu}_x \rangle}{\langle \hat{I}_x \rangle} = [g_{l,\pi} \langle \hat{j}_{\pi,x} \rangle + (g_{s,\pi} - g_{l,\pi}) \langle \hat{S}_{\pi,x} \rangle$$
$$+ g_{s,\nu} \langle \hat{S}_{\nu,x} \rangle]/I, \quad (3)$$

where $\langle \hat{j}_{\pi,x} \rangle$, $\langle \hat{S}_{\pi,x} \rangle$, and $\langle \hat{S}_{\nu,x} \rangle$ are expectation values of the total spin or intrinsic spin projections on the cranking axis of protons and neutrons. Throughout this work we have used $g_s = 0.7 g_s^{\mathrm{free}}$.

III. ISOMERIC STATES IN ^{178}Hf

The CNSB potential energy surfaces (PESs) for the ground and isomeric states of ^{178}Hf are displayed in Fig. 1. At the ground state with $K^\pi = 0^+$ and also at $K^\pi = 6^+$, a collective main minimum appears at $\varepsilon_2 \approx 0.26$ and $\gamma \approx 0°$. However, it is shown in Ref. [30] that the $K^\pi = 6^+$ state is not an yrast state and decays to the 6^+ member of the ground-state band (6^+_{GSB}) with $E_\gamma = 0.922$ MeV. Note that in the calculation a
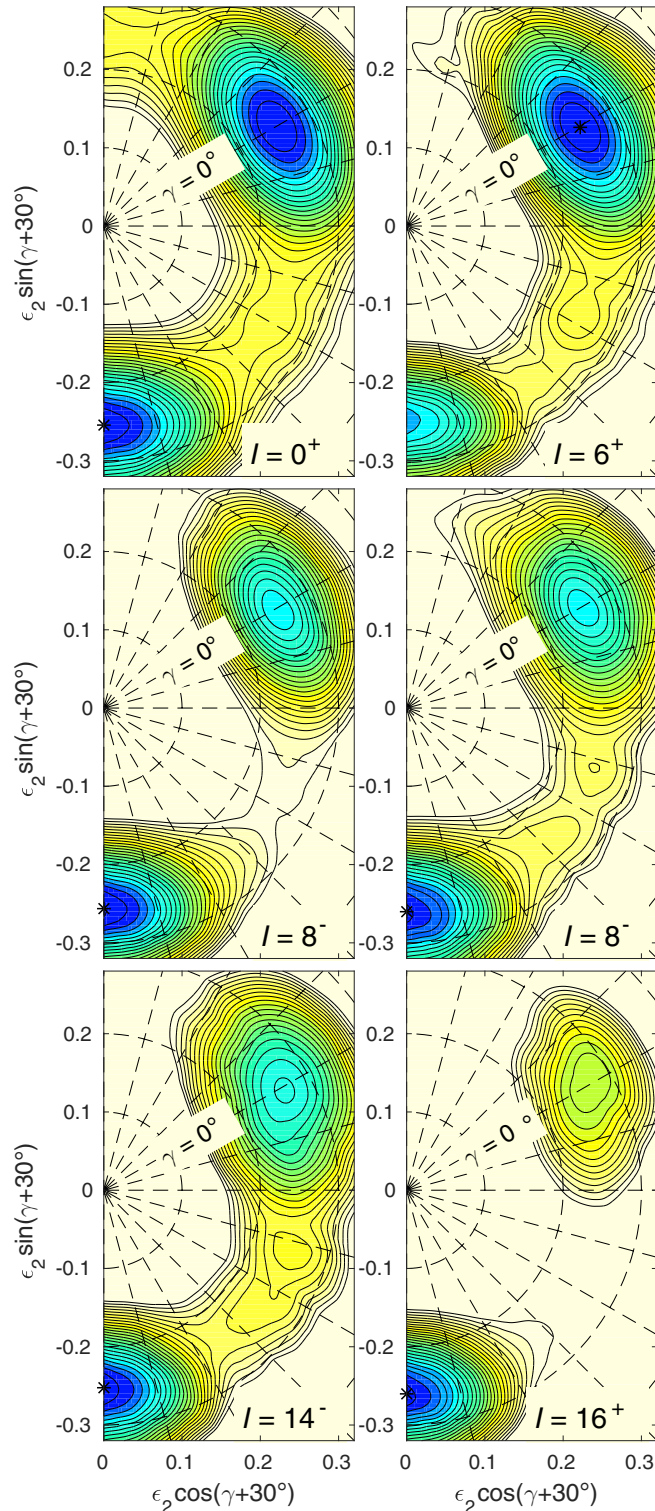
FIG. 1. Calculated CNSB potential-energy surfaces versus quadrupole deformation ε_2 and the triaxiality parameter γ of ^{178}Hf for the $I = 0$ ground state, $I = 6^+$ states (see text), $I = 8^-$ proton isomer (left), $I = 8^-$ neutron isomer (right), and also $I = 14^-$ and 16^+ isomers. Contour lines are separated by 0.25 MeV and the γ plane is marked at $15°$ intervals. Dark regions represent low energy and absolute minima are labeled with dots.
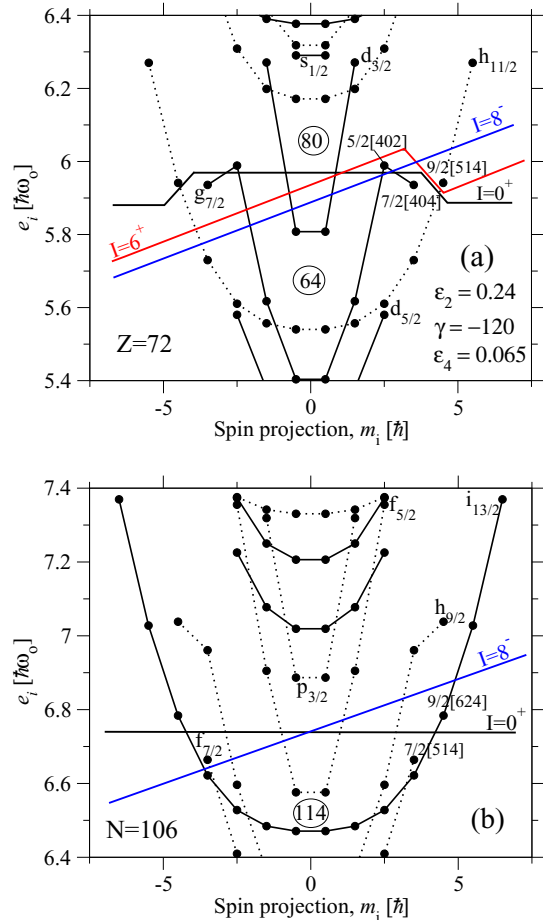

FIG. 2. Single-particle energies e_i for a prolate shape, $\varepsilon_2 = 0.240$, $\gamma = -120°$, $\varepsilon_4 = 0.065$, versus spin projection on the symmetry axis m_i, for (a) protons and (b) neutrons in ^{178}Hf. Energies (y axis) are in oscillator units. Tilted Fermi surfaces indicate the filling of the orbitals in the aligned $I_p = 6^+$ and 8^- and also $I_n = 8^-$ states.

noncollective state with $\gamma = -120°$ represents the $K^\pi = 6^+$ state and coexists with the collective GSB state, which is at slightly lower energy (by about 0.8 MeV). The calculations show that the 6^+ isomer, just as other isomers in ^{178}Hf, appears as a multiquasiparticle prolate mode with $\gamma = -120°$, as presented in Table I.

The calculations for the $K^\pi = 8^-$ state show the yrast state at $\varepsilon_2 \approx 0.26$ and $\gamma \approx -120°$, indicating a noncollective prolate shape corresponding to a two-quasineutron and two-quasiproton structure. A less favored prolate minimum is also observed at $\varepsilon_2 \approx 0.26$ and $\gamma \approx 0°$. Similar PESs are also obtained for the $K^\pi = 14^-$ and $K^\pi = 16^+$ states. The calculations indicate significant hexadecapole deformations with ε_4 in the range 0.05–0.06.

A more quantitative comparison between different aligned configurations is obtained from the CNS single-particle energies, e_i versus m_i diagrams drawn at the appropriate deformation. The most favored states are selected by filling the pure CNS orbitals below the straight line tilted Fermi surfaces illustrated in Fig. 2 for $Z = 72$ and $N = 106$. Spins

TABLE I. Calculated and experimental values of excitation energies and g factors, and calculated pairing energies and isomeric state configurations in ^{178}Hf. Energies are in MeV. Experimental data are taken from Ref. [34].

K^π	ε_2	γ	ε_4	E_{the}	E_{exp}	$E_{the}[8]$	g_{the}	g_{exp}	E_{pair}	I_p/I	Proton configuration	Neutron configuration
0^+	0.255	$-120°$	0.050	0	0	0	–	–	2.717	0	GS	GS
6^+	0.255	$-120°$	0.050	1.439	1.554	–	1.032	0.97	1.395	1	$\left[\frac{5}{2}^+[402]\frac{7}{2}^+[404]\right]_{6^+}$	–
8^-	0.256	$-120°$	0.055	1.151	1.147	1.348	0.344	0.39	1.550	1	$\left[\frac{7}{2}^+[404]\frac{9}{2}^-[514]\right]_{8^-}$	–
8^-	0.261	$-120°$	0.054	1.317	1.479	–	0.635	–	2.039	0	–	$\left[\frac{7}{2}^-[514]\frac{9}{2}^+[624]\right]_{8^-}$
14^-	0.253	$-120°$	0.049	2.916	2.572	–	0.428	0.60	1.284	0.429	$\left[\frac{5}{2}^+[402]\frac{7}{2}^+[404]\right]_{6^+}$	$\left[\frac{7}{2}^-[514]\frac{9}{2}^+[624]\right]_{8^-}$
16^+	0.261	$-120°$	0.058	2.541	2.446	2.401	0.490	0.51	1.213	0.50	$\left[\frac{7}{2}^+[404]\frac{9}{2}^-[514]\right]_{8^-}$	$\left[\frac{7}{2}^-[514]\frac{9}{2}^+[624]\right]_{8^-}$

can be obtained from particle-hole excitations relative to the tilted Fermi surface [18]. For ^{178}Hf, e_i versus m_i diagrams are plotted at the deformation $(\varepsilon_2, \gamma, \varepsilon_4) \approx (0.24, -120°, 0.065)$ for protons and neutrons in Figs. 2(a) and 2(b), respectively, where the corresponding isomer structures are shown schematically. The single-particle energies are drawn at a moderate deformation because one can use the diagrams also for other isotopes.

As seen in Fig. 2(b), the $K^\pi = 8^-$ state can be built by moving a neutron from the $f_{7/2}$ orbital with $m = -7/2$, above the tilted Fermi level, to the $i_{13/2}$ orbital with $m = 9/2$, below the tilted Fermi level. Similarly, in Fig. 2(a), the 8^- state can be made by transferring a proton from the $h_{11/2}$ orbital ($m = 9/2$), to the $g_{7/2}$ orbital ($m = 7/2$). Therefore, it may be concluded that the structure of the 8^- isomeric state has the $\pi\frac{7}{2}^+[404], \frac{9}{2}^-[514]$ or the $\nu\frac{7}{2}^-[514], \frac{9}{2}^+[624]$ two-quasiparticle configuration. Experiments have revealed that the 8^- state is a mixture of these two structure types with a dominant two-quasineutron admixture in the isomer band [30].

For making the $K^\pi = 6^+$ state, it is necessary to transfer a proton from the $g_{7/2}$ orbital with $m = 7/2$ to $m = 5/2$, forming the two-quasiproton configuration $\pi\frac{5}{2}^+[402], \frac{7}{2}^+[404]$. The configuration obtained for the 6^+ state is consistent with the result in Ref. [30], while it is in contrast to the result in Ref. [31] where the 6^+ state is described as a two-quasineutron configuration $\nu\frac{5}{2}^-[512], \frac{7}{2}^-[514]$ within the the projected shell model [32]. As seen in Fig. 2, our calculations show that moving a neutron from the $h_{11/2}$ orbital with $m = 5/2$ to $m = 7/2$ needs more energy than moving a proton from the $g_{7/2}$ orbital with $m = 7/2$ to $m = 5/2$. On the other hand, the 6^+ state was suggested to have a combined structure with 69% $\pi\frac{7}{2}^+[404], \frac{5}{2}^+[402]$ plus 31% $\nu\frac{7}{2}^-[514], \frac{5}{2}^-[512]$ [33]. However, it is concluded in Ref. [30] that the 6^+ state is predominantly of two-quasiproton character, which is consistent with our results.

The isomeric $K^\pi = 14^-$ state includes the proton spin $I_p^\pi = 6^+$ with the configuration $\pi\frac{5}{2}^+[402], \frac{7}{2}^+[404]$ and the neutron spin $I_n^\pi = 8^-$ with the configuration $\nu\frac{7}{2}^-[514], \frac{9}{2}^+[624]$. Also, Fig. 2 shows that the isomeric $K^\pi = 16^+$ state is built by combining the two suggested configurations for the 8^- state, $\pi\frac{7}{2}^+[404], \frac{9}{2}^-[514], \nu\frac{7}{2}^-[514], \frac{9}{2}^+[624]$. Therefore the 14^- and 16^+ isomers are built on four-quasiparticle configurations.

It is possible also to check the number of quasiparticles in the CNSB procedure. Our calculations for the yrast 8^-, 14^-, and 16^+ isomers confirm that the 8^- isomer is a two-quasiparticle state and the 14^- and 16^+ isomers are four-quasiparticle states. The calculations reveal that there are no quasiparticles in the 6^+ yrast state with the $(\pi_p, \alpha_p)(\pi_n, \alpha_n) = (+, 0)(+, 0)$ configuration, where π is the parity and α is the signature. Therefore, we have to put two quasiprotons in the configuration $(+, 0)(+, 0)$ to get an isomeric $K^\pi = 6^+$ state with two quasiparticles. Our calculations predict for $6^+_{isomer} \rightarrow 6^+_{GSB}$ a transition energy of about 0.668 MeV which is not far from the experimental value of 0.922 MeV [30].

Table I shows the configuration assigned for each isomer in ^{178}Hf. We have also calculated the excitation energies for the isomeric states and compared them with the experimental values and theoretical ones obtained from the TRS model [8] in Table I. For the 8^- isomer, the g factor of the mixture of the two 8^- configurations is calculated assuming 36% and 64% of the pure proton and neutron states, respectively [30]. The pure values are 1.01 and -0.03 for the proton and neutron 8^- configurations, respectively. We have also determined the g factors, and the proportion of the spin from protons for each state, in the CNSB calculations which are listed in Table I. Comparison of the experimental and calculated values in Table I shows that the present formalism is able to reproduce the major features of the isomers.

For better understanding of the isomer structures, we have calculated the pairing energy E_{pair} for each isomeric state as the difference of the unpaired CNS and paired CNSB energies. They are included in Table I, where it is seen that the pairing energy decreases with increasing quasiparticle number, as we expect. It also shows that the pairing energy for the 8^- state with two quasineutrons is more than that of the 8^- state with two quasiprotons. This is because the quasineutrons occupy orbitals with larger l and j values in comparison with the occupied orbitals in the two-quasiproton state. The value $\frac{I_p}{I} = 1$ for the 6^+ and 8^- two-quasiproton states confirms they are built on pure quasiproton structures with no quasineutron contributions. Also the proton spin proportion of the 16^+ state equals 0.5, which indicates it is built on two quasiprotons and two quasineutrons with the same spin proportions, while for the 14^- state, it equals 0.429 which is consistent with $I_p = 6$ and $I_n = 8$.

The results show that the present model can capture the important properties of the isomeric states in ^{178}Hf. The model

TABLE II. Calculated and experimental values of the deformation, excitation energy, and the structure of the multiquasiparticle states in ^{180,182,184,186}Hf. Energies are in MeV. Experimental data for the excitation energies are taken from Refs. [34,35].

Isotopes	K^π	ε_2	γ	ε_4	E_{the}	E_{exp}	E_{the}[8]	Proton configuration	Neutron configuration
^{180}Hf	0^+	0.251	$-120°$	0.063	0	0	0	GS	GS
	4^-	0.249	$-120°$	0.062	1.143	1.374	−	−	$\left[\frac{1}{2}^-[521]\frac{9}{2}^+[624]\right]_{4^-}$
	6^+	0.249	$-120°$	0.064	1.574	1.702	−	$\left[\frac{5}{2}^+[402]\frac{7}{2}^+[404]\right]_{6^+}$	−
	8^-	0.252	$-120°$	0.066	1.077	1.143	1.303	$\left[\frac{7}{2}^+[404]\frac{9}{2}^-[514]\right]_{8^-}$	−
	10^+	0.248	$-120°$	0.064	2.109	2.424	−	−	$\left[\frac{9}{2}^+[624]\frac{11}{2}^+[615]\right]_{10^+}$
	12^+	0.251	$-120°$	0.064	2.298	2.484	2.462	$\left[\frac{7}{2}^+[404]\frac{9}{2}^-[514]\right]_{8^-}$	$\left[\frac{9}{2}^+[624]\frac{1}{2}^-[521]\right]_{4^-}$
	14^+	0.251	$-120°$	0.066	2.513	2.805	−	$\left[\frac{7}{2}^+[404]\frac{9}{2}^-[514]\right]_{8^-}$	$\left[\frac{9}{2}^+[624]\frac{3}{2}^-[512]\right]_{6^-}$
	18^-	0.246	$-120°$	0.064	3.696	3.595	−	$\left[\frac{7}{2}^+[404]\frac{9}{2}^-[514]\right]_{8^-}$	$\left[\frac{9}{2}^+[624]\frac{11}{2}^+[615]\right]_{10^+}$
^{182}Hf	0^+	0.241	$-120°$	0.067	0	0	0	GS	GS
	8^-	0.243	$-120°$	0.070	1.057	1.173	1.268	$\left[\frac{7}{2}^+[404]\frac{9}{2}^-[514]\right]_{8^-}$	−
	13^+	0.241	$-120°$	0.070	2.862	2.573	2.652	$\left[\frac{7}{2}^+[404]\frac{9}{2}^-[514]\right]_{8^-}$	$\left[\frac{11}{2}^+[615]\frac{1}{2}^-[510]\right]_{5^-}$
^{184}Hf	0^+	0.228	$-120°$	0.069	0	0	0	GS	GS
	8^-	0.234	$-120°$	0.076	1.058	1.264	1.232	$\left[\frac{7}{2}^+[404]\frac{9}{2}^-[514]\right]_{8^-}$	−
	15^+	0.233	$-120°$	0.081	2.668	2.477	2.266	$\left[\frac{7}{2}^+[404]\frac{9}{2}^-[514]\right]_{8^-}$	$\left[\frac{3}{2}^-[512]\frac{11}{2}^+[615]\right]_{7^-}$
^{186}Hf	0^+	0.200	$-120°$	0.060	0	0	0	GS	GS
	8^-	0.209	$-120°$	0.063	1.170	−	1.170	$\left[\frac{7}{2}^+[404]\frac{9}{2}^-[514]\right]_{8^-}$	−
	10^-	0.193	$-120°$	0.059	1.658	−	−	−	$\left[\frac{9}{2}^-[505]\frac{11}{2}^+[615]\right]_{10^-}$
	17^+	0.213	$-120°$	0.079	2.479	2.968	2.088	$\left[\frac{7}{2}^+[404]\frac{9}{2}^-[514]\right]_{8^-}$	$\left[\frac{11}{2}^+[615]\frac{7}{2}^-[503]\right]_{9^-}$
	18^+	0.207	$-120°$	0.071	3.020	−	2.686	$\left[\frac{7}{2}^+[404]\frac{9}{2}^-[514]\right]_{8^-}$	$\left[\frac{9}{2}^-[505]\frac{11}{2}^+[615]\right]_{10^-}$

can be generalized to determine also the features of other isomers. In the following, we extend the calculations to the heavier hafnium isotopes.

IV. ISOMERIC STATES IN ^{180,182,184,186}Hf

Here, we have studied the isomeric state properties in four even-even neutron-rich hafnium isotopes, ^{180,182,184,186}H by the same procedure as for ^{178}Hf described in the previous section. Seven multiquasiparticle states are experimentally observed in ^{180}Hf, with $K^\pi = 4^-, 6^+, 8^-, 10^+, 12^+, 14^+$, and 18^- [34,35], two isomeric states in ^{182}Hf, with $K^\pi = 8^-$ and 13^+ [34,36], two isomeric states in ^{184}Hf, with $K^\pi = 8^-$ and 15^+ [16,34], and one isomeric state in ^{186}Hf, with $K^\pi = 17^+$ [16,34]. The calculated deformations and excitation energies of the isomeric states are presented in Table II. They are found to have prolate shape with $\varepsilon_2 \approx 0.25 - 0.21$, $\gamma = -120°$, and $\varepsilon_4 \approx 0.06 - 0.08$. As expected, all isomers are built from multiquasiparticle prolate orbitals.

In ^{180}Hf, just as in ^{178}Hf, the two-quasiparticle 6^+ isomer is not an yrast state, and it decays to the GSB 6^+ state with a transition energy of 1.062 MeV [35]. The 4^- and 8^- two-quasiparticle isomers form negative-parity yrast states. There are four-quasiparticle isomers with $K^\pi = 12^+$ and 18^- [35].

Our findings on the energies of multiquasiparticle states are compared with experimental data [34,35] in Table II and also with the theoretical results reported in Ref. [8], where the calculations are done within the macroscopic-microscopic model based on the deformed Woods-Saxon potential plus the Lipkin-Nogami (LN) treatment of pairing [37]. They have

investigated the two-quasiproton 8^- isomers and some four-quasiparticle isomers in even-even hafnium isotopes [8]. The isomeric $K^\pi = 8^-$ state is predicted in all the neutron-rich hafnium isotopes with the configuration $\pi \frac{7}{2}^+[404]$, $\frac{9}{2}^-[514]$, as is evident in Fig. 2(a).

The quasiparticle structures of the isomeric states are determined by drawing the single-particle energies e_i versus spin projection on the symmetry axis m_i as shown in Fig. 3, that lead us to the single-particle contributions of the neutrons, while the protons are shown in Fig. 2(a). The $K^\pi = 6^+$ and 8^- states in ^{180}Hf have the same proton structures as those discussed in ^{178}Hf, as indicated in Fig. 2(a) (though, as discussed, there is proton-neutron mixing in the 8^- state of ^{178}Hf). As seen in Fig. 3(a), the $i_{13/2}$ neutron with $m = 9/2$ contributes to creating the spin $I_n = 4^-, 6^-$, and 10^+ states by promoting a neutron to the $p_{3/2}(m = -1/2)$, $f_{5/2}(m = 3/2)$, and $i_{13/2}(m = 11/2)$ orbitals, respectively. They can also combine with the $I_p = 8^-$ configuration [see Fig. 2(a)] to form the $K^\pi = 12^+, 14^+$, and 18^- states in ^{180}Hf.

Figure 3(b) indicates that the $\frac{11}{2}^+[615]$ member of the $i_{13/2}$ neutron orbitals is responsible for forming the neutron spins $I_n = 5^-, 7^-$, and 9^- when occupied by an aligned neutron from the $p_{3/2}$ $(m = -1/2)$, $f_{5/2}$ $(m = 3/2)$, and $h_{9/2}$ $(m = 7/2)$ orbitals, respectively. They can combine with the proton $I_p = 8^-$ state to form the $K^\pi = 13^+, 15^+$, and 17^+ four-quasiparticle states with neutron numbers $N = 110, 112$, and 114, respectively.

Experimental energies and structures of the isomers in ^{180,182,184,186}Hf are listed in Table II. One can see that the present model reproduces quite well the experimental
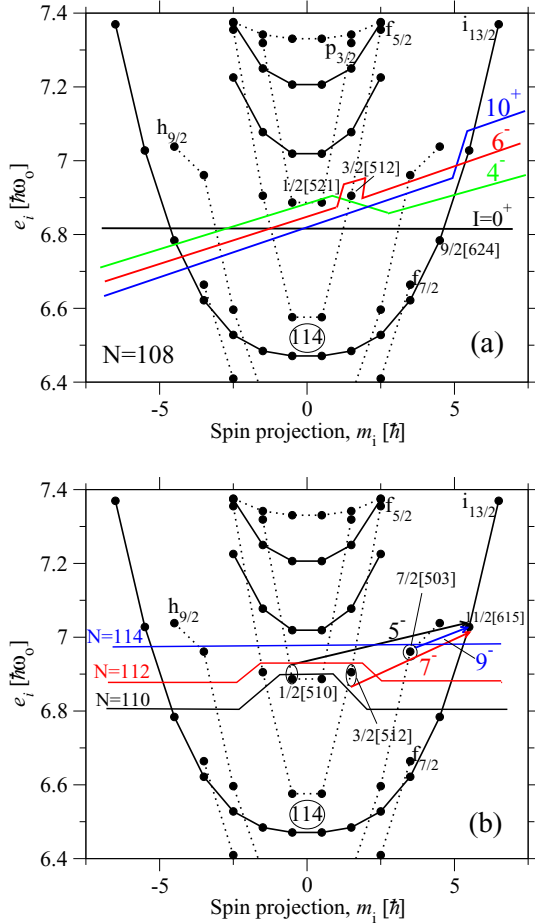
FIG. 3. Single-neutron energies e_i for a prolate shape, $\varepsilon_2 = 0.240$, $\gamma = -120°$, $\varepsilon_4 = 0.065$, versus spin projection on the symmetry axis m_i. Energies (y axis) are in oscillator units. (a) For $N = 108$, the tilted Fermi surfaces indicate the filling of the orbitals in the aligned $I_n = 4^-$, 6^-, and 10^+ states. (b) For $N = 110$, 112, and 114, the arrows show which neutron is promoted to the $\frac{11}{2}^+$[615] orbital to create $I_n = 5^-$, 7^-, and 9^- configurations.

observations, as well as the results given by other calculations [16,35,38].

Based on the favored 8^- state for $Z = 72$, we predict an 8^- isomer also in ^{186}Hf, with the energy 1.170 MeV in a good agreement with Ref. [8]. Also observed theoretically is a 10^- state formed by moving two neutrons from the orbital $h_{9/2}$ ($m = \pm7/2$) to the $h_{9/2}$ ($m = 9/2$) and $i_{13/2}$ ($m = 11/2$), which is only about 0.49 MeV higher than the two-quasiproton 8^- state in energy. One can also predict a four-quasiparticle 18^+ state with the energy 3.020 MeV in ^{186}Hf. These isomers which have not yet been identified experimentally, are presented in Table II.

V. HIGH-SPIN SHAPE COEXISTENCE

To predict the existence of the isomers at high spin, it is necessary to see whether the multiquasiparticle states are yrast also in the high-spin region. It was shown that hafnium high-K multiquasiparticle excitations can be lower in energy than the

prolate collective states over a range of angular momentum [39]. On the other hand, a collective prolate-oblate shape change is predicted in the neutron-rich hafnium isotopes, with lower energy for the oblate collective mode in the high-spin region [15,40]. Here, we have studied the CNSB PESs of neutron-rich hafnium isotopes at high spins to find the favored states with increasing angular momentum within the present method.

Figure 4 demonstrates the PESs of the $(\pi, \alpha)_p(\pi, \alpha)_n = (+, 0)(+, 0)$ configuration in ^{180}Hf at $I = 0$, 14, 28, and 36. Our studies show that the general behavior, as seen in Fig. 4, is representative of the neutron-rich hafnium isotopes. In the low-spin region, the collective and multiquasiparticle (noncollective) prolate minima are favored. With increasing spin, the noncollective prolate mode becomes energetically lower than the collective prolate mode so that multiquasiparticle states with $\gamma = -120°$ become yrast. However, at high spin, a well-deformed oblate rotation minimum appears which becomes yrast with increasing spin at about $I = 36$. The spin at the transition between the noncollective prolate and collective oblate modes depends on the neutron number as well as the $(\pi, \alpha)_p(\pi, \alpha)_n$ configuration. This transition occurs at $I \approx 40$ for the $(+, 0)(-, 0)$ configuration in ^{180}Hf and ^{182}Hf, while it occurs at $I \approx 34$ for the $(+, 0)(+, 0)$ configuration in ^{186}Hf. Figure 4 indicates also some local minima around $\gamma \approx 0°$. As mentioned, a similar trend is observed in the PESs of a range of heavy hafnium isotopes ($A \geqslant 178$) with increasing spin. The present calculations show that the oblate, or approximately oblate, rotational mode at $\gamma \approx -60°$ gradually appears with increasing spin and competes strongly with the noncollective prolate states, becoming yrast at higher spins, $I = 30-40$. The observed shape evolution and transition from collective to noncollective modes agree with the findings in Ref. [15], where the favored states are investigated with increasing rotational frequency in ^{182,186}Hf. A different trend is revealed in the lighter isotopes, such as ^{168}Hf, where prolate rotation with $\varepsilon_2 \approx 0.23$ at low and medium spins becomes triaxial with increasing spin, as seen in Fig. 5 of Ref. [29].

We note that, for prolate shapes in the neutron-rich hafnium isotopes, both proton and neutron Fermi surfaces are close to high-Ω, high-j orbitals, favoring deformation-aligned high-K isomers ($\gamma = -120°$), whereas for oblate shapes both Fermi surfaces are amongst low-Ω, high-j orbitals, so that angular momentum can be efficiently generated by rotational alignment with the oblate shape ($\gamma = -60°$). It is these two modes that compete for yrast status at high spin.

In the CNSB method, it is possible to limit the minimization around selected deformations. In such a way, we have investigated the prolate-oblate competition in the hafnium isotopes with $A = 178-188$ to see how these modes compete over a wide range of spin. The energies of yrast and near-yrast states for the prolate collective, prolate noncollective, and oblate collective modes are plotted for the $^{178-188}$Hf isotopes in Fig. 5, shown by the black, red, and blue lines, respectively, for spins $I = 0 - 40$. Yrast status was found for all $(\pi, \alpha)_p(\pi, \alpha)_n$ configurations, as a function of spin. Note that Fig. 4 is drawn for only one (π, α) configuration, hence, one can expect to see differences between this figure and Fig. 5.
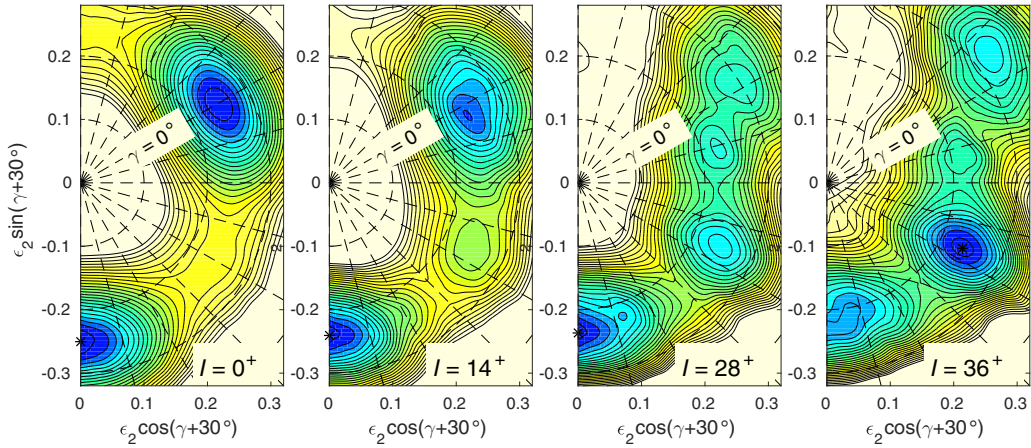
FIG. 4. Calculated CNSB potential-energy surfaces versus quadrupole deformation ε_2 and the triaxiality parameter γ of ^{180}Hf with $(\pi, \alpha) = (+, 0)$ for spins $I = 0$, 14, 28, and 36. Contour lines are separated by 0.25 MeV and the γ plane is marked at $15°$ intervals. Dark regions represent low energy with absolute minima shown as dots.

As seen in Fig. 5, in all illustrated hafnium isotopes, the yrast states are prolate collective at low spin, and multiquasiparticle prolate noncollective at intermediate spin. The oblate collective structure competes strongly with the prolate noncollective structure at high spins. For example, in ^{186}Hf at $I = 38$ the prolate noncollective yrast state is lower energetically than the oblate-collective state by only about 0.02 MeV. We note that, in ^{180}Hf, experimental evidence was found for the oblate collective mode becoming energetically favored over the prolate collective mode at $I^\pi = 20^+$ [41].

In Fig. 5, we have also drawn the energy of the ground-state bands (GSB) and the isomer states relative to the rotating liquid drop energy for the available isotopes. It is seen that the experimental GSB and isomer states compare well with the collective ($\gamma = 0°$) and the noncollective ($\gamma = 120°$) prolate states, respectively, as explained in Secs. III and IV. Note that the present formalism is based on principal axis cranking where the total spin is counted along the rotation axis. Therefore, comparing the CNSB yrast lines with the rotational bands built on the high-K isomers can be doubtful, and instead
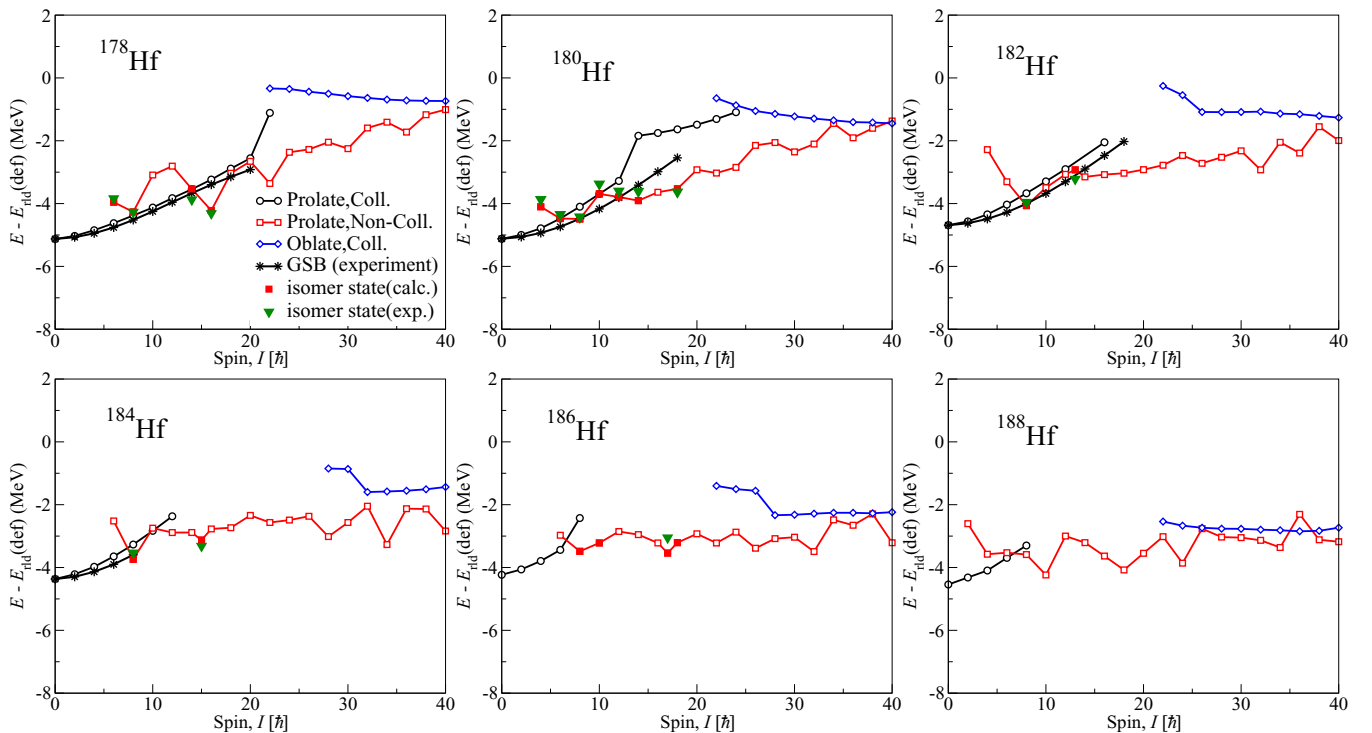

FIG. 5. The calculated energies of the prolate collective (black circles), prolate noncollective (red squares), and the oblate collective (blue diamonds) states for $^{178-188}$Hf, and the experimental energies of the ground-state band (GSB) of $^{178-184}$Hf (black stars) are shown relative to the rotating liquid drop energy. The experimental data are taken from Refs. [42–44]. Also shown are the calculated (filled red squares) and the experimental (filled green triangles) isomer states.

the calculation may be done within a tilted axis cranking (TAC) model [45].

VI. SUMMARY

We have interpreted the isomer structures in even-even hafnium isotopes with $A = 178$–186 based on the unpaired CNS and the paired CNSB formalisms. The calculated excitation energies as well as the configurations of the isomers have been compared with the experimental findings and also the TRS model, and good agreements are observed.

The calculations reveal that the collective prolate and non-collective prolate states are favored at low and medium spins, respectively, in hafnium isotopes. At $I \geqslant 35$, collective oblate rotation leads to a deep potential minimum, and it strongly competes with the noncollective prolate states to become yrast.

The present study is the first attempt to describe the structure of multiquasiparticle isomers using the CNS and CNSB methods. Our results show that the present method can be employed successfully to analyze the experimental findings, opening the way to further investigation of this neutron-rich region of high-spin, long-lived isomers.

[1] P. M. Walker and G. D. Dracoulis, Nature (London) **399**, 35 (1999).

[2] G. D. Dracoulis, P. M. Walker, and F. G. Kondev, Rep. Prog. Phys. **79**, 076301 (2016).

[3] G. D. Dracoulis, Phys. Scr. **2013**, 014015 (2013).

[4] P. M. Walker, Nucl. Phys. A **834**, 22c (2010).

[5] C. F. Von Weizsäcker, Naturwissenschaften **24**, 813 (1936).

[6] C. S. Purry, P. M. Walker, G. D. Dracoulis, T. Kibédi, S. Bayer, A. M. Bruce, A. P. Byrne, M. Dasgupta, W. Gelletly, F. Kondev, P. H. Regan, and C. Thwaites, Phys. Rev. Lett. **75**, 406 (1995).

[7] F. Browne *et al.*, Phys. Rev. C **96**, 024309 (2017).

[8] H. L. Liu, F. R. Xu, P. M. Walker, and C. A. Bertulani, Phys. Rev. C **83**, 067303 (2011).

[9] X. Y. Wu, S. K. Ghorui, L. J. Wang, Y. Sun, M. Guidry, and P. M. Walker, Phys. Rev. C **95**, 064314 (2017).

[10] H. L. Liu, P. M. Walker, and F. R. Xu, Phys. Rev. C **89**, 044304 (2014).

[11] R. T. Wood *et al.*, Phys. Rev. C **95**, 054308 (2017).

[12] F. S. Stephens and R. S. Simon, Nucl. Phys. A **183**, 257 (1972).

[13] C. B. Collins *et al.*, Phys. Rev. Lett. **82**, 695 (1999).

[14] M. B. Smith, P. M. Walker, G. C. Ball, J. J. Carroll, P. E. Garrett, G. Hackman, R. Propri, F. Sarazin, and H. C. Scraggs, Phys. Rev. C **68**, 031302(R) (2003).

[15] F. R. Xu, P. M. Walker, and R. Wyss, Phys. Rev. C **62**, 014301 (2000).

[16] M. W. Reed, P. M. Walker, I. J. Cullen, Y. A. Litvinov, D. Shubina, G. D. Dracoulis *et al.*, Phys. Rev. C **86**, 054321 (2012).

[17] P. M. Walker and Zs. Podolyák, Phys. Scr. **95**, 044004 (2020).

[18] A. V. Afanasjev, D. B. Fossan, G. J. Lane, and I. Ragnarsson, Phys. Rep. **322**, 1 (1999).

[19] T. Bengtsson and I. Ragnarsson, Nucl. Phys. A **436**, 14 (1985).

[20] B. G. Carlsson and I. Ragnarsson, Phys. Rev. C **74**, 011302(R) (2006).

[21] B. G. Carlsson, I. Ragnarsson, R. Bengtsson, E. O. Lieder, R. M. Lieder, and A. A. Pasternak, Phys. Rev. C **78**, 034316 (2008).

[22] H.-L. Ma, B. G. Carlsson, I. Ragnarsson, and H. Ryde, Phys. Rev. C **90**, 014316 (2014).

[23] T. Bengtsson, Nucl. Phys. A **496**, 56 (1989).

[24] T. Bengtsson, R. A. Broglia, E. Vigezzi, F. Barranco, F. Dönau, and Jing-ye Zhang, Phys. Rev. Lett. **62**, 2448 (1989).

[25] S. G. Nilsson and I. Ragnarsson, *Shapes and Shells in Nuclear Structure* (Cambridge University Press, Cambridge, 2005).

[26] K. Pomorski and J. Dudek, Phys. Rev. C **67**, 044316 (2003).

[27] V. M. Strutinsky, Nucl. Phys. A **122**, 1 (1968).

[28] T. Bengtsson, Nucl. Phys. A **512**, 124 (1990).

[29] A. Kardan, I. Ragnarsson, H. Miri-Hakimabad, and L. Rafat-Motevali, Phys. Rev. C **86**, 014309 (2012).

[30] A. B. Hayes, D. Cline, C. Y. Wu, H. Ai, H. Amro, C. Beausang *et al.*, Phys. Rev. C **75**, 034308 (2007).

[31] Y. Sun *et al.*, Phys. Lett. B **589**, 83 (2004).

[32] K. Hara and Y. Sun, Int. J. Mod. Phys. E **4**, 637 (1995).

[33] T. L. Khoo and G. Løvhøiden, Phys. Lett. B **67**, 271 (1977).

[34] A. K. Jain *et al.*, Nucl. Data sheets **128**, 1 (2015).

[35] S. K. Tandel, P. Chowdhury, F. G. Kondev, R. V. F. Janssens, T. L. Khoo, M. P. Carpenter *et al.*, Phys. Rev. C **94**, 064304 (2016).

[36] R. D'Alarcao *et al.*, Phys. Rev. C **59**, R1227(R) (1999).

[37] H. C. Pradhan, Y. Nogami, and J. Law, Nucl. Phys. A **201**, 357 (1973).

[38] M. W. Reed, I. J. Cullen, P. M. Walker, Y. A. Litvinov, K. Blaum, F. Bosch *et al.*, Phys. Rev. Lett. **105**, 172501 (2010).

[39] S. Åberg, Nucl. Phys. A **306**, 89 (1978).

[40] R. R. Hilton and H. J. Mang, Phys. Rev. Lett. **43**, 1979 (1979).

[41] U. S. Tandel *et al.*, Phys. Rev. Lett. **101**, 182503 (2008).

[42] A. B. Hayes, D. Cline, C. Y. Wu, M. W. Simon, R. Teng *et al.*, Phys. Rev. Lett. **89**, 242501 (2002).

[43] E. Ngijoi-Yogo, S. K. Tandel, G. Mukherjee, I. Shestakova, P. Chowdhury *et al.*, Phys. Rev. C **75**, 034305 (2007).

[44] K. Krumbholz, W.-D. Schmidt-Ott, T. Hild, V. Kunze, F. Meissner *et al.*, Z. Phys. A **351**, 11 (1995).

[45] S. Frauendorf, Rev. Mod. Phys. **73**, 463 (2001).